HHS Public Access

Author manuscript

Small. Author manuscript; available in PMC 2015 September 24.

Published in final edited form as:

Small. 2014 September 24; 10(18): 3729–3734. doi:10.1002/smll.201400733.

Molecular Imaging Using Nanoparticle Quenchers of Cerenkov Luminescence

Daniel L.J. Thorek [Assistant Prof],

Division of Nuclear Medicine, Department of Radiology and Radiological Sciences, The Johns Hopkins School of Medicine, Baltimore, MD, 21205

Sudeep Das [Research Fellow], and

Program in Molecular Pharmacology and Chemistry, Memorial Sloan-Kettering Cancer Center, New York, New York, 10021. USA

Jan Grimm[*] **[Assistant Prof]**

Program in Molecular Pharmacology and Chemistry, Memorial Sloan-Kettering Cancer Center, New York, New York, 10021. USA.

Abstract

Cerenkov luminescence (CL) imaging is an emerging technique that collects the visible photons produced by radioisotopes. Here, we have investigated molecular imaging strategies by modulating CL signal off. Utilizing a combination of clinically approved agents, and their analogues, we demonstrate the noninvasive molecularly specific detection of cancer. CL was modulated *in vitro* in a dose dependent manner using approved small molecules (Lymphazurin), as well as the clinically approved Feraheme and other preclinical superparamagnetic iron oxide nanoparticles (SPIO). To evaluate the quenching of CL *in vivo*, two strategies were pursued. [^{18}F]-FDG was imaged by PET and CL in tumors prior to and following accumulation of nanoparticles. Initially, non-targeted particles were administered to mice bearing tumors in order to attenuate CL. For targeted imaging, a dual tumor model (expressing the human somatostatin receptor subtype-2 (hSSTr2) and a control negative cell line) was used. Targeting hSSTr2 with octreotate-conjugated SPIO, we demonstrate quenched CL enabling non-invasive distinction between tumors' molecular expression profiles. In this work, we demonstrate quenching of Cerenkov emissions in several proof of principle models using a combination of approved agents and nanoparticle platforms to provide disease relevant information including tumor vascularity and specific antigen expression.

Keywords

molecular targeting; quenching nanoparticles; activatable imaging; Cerenkov luminescence; Activatable Cerenkov Luminescence

[*]grimmj@mskcc.org..

Supporting Information

Supporting Information is available from the Wiley Online Library or from the author.

1. Introduction

Molecular imaging plays an increasingly important role in basic research, preclinical evaluation and patient management. The diverse modalities possess a wide range of sensitivities, depths of penetration, resolution, throughput and cost.[1] Optical molecular imaging, primarily through microscopy applications, is the predominant technique for laboratory investigation.

Optical imaging provides relatively low cost, high resolution of cells and excised tissues, as well as intact animals. A plethora of luminescent, bioluminescent and fluorescent agents have been studied in the past two decades. These provide basic researchers with a wealth of probes that hold great promise to better interrogate the molecular and cellular basis of disease.[2] However, despite their success at the benchtop, clinical impact of these agents has been lacking. To the best of our knowledge there are only two fluorescent agents with clinical indications (sodium fluorescein and indocyanine green). While there are recent exceptions in specialized settings[3] light's limited depth penetration and questions regarding toxicity and pharmacodynamics of agents are key impediments to greater use.

Conversely, through its tracer approach, high resolution, depth independent and quantitative nature, positron emission tomography (PET) is an essential tool in both pre- and clinical imaging. A recent development has been the acquisition of Cerenkov radiation from PET isotopes for optical imaging. Cerenkov radiation is the light generated when charged particles (e.g. β^- and β^+ particles emitted upon radioactive decay) exceed the speed of light in a dielectric medium (**Figure 1A**). First observed over a century ago,[4] visualization of this radiation *in vivo*, termed Cerenkov luminescence (CL), has only recently been achieved.[5] The multiple advantages of CL include higher throughput capabilities, greater surface resolution and cost savings as compared to PET. As CL can utilize clinical approved tracers[6] it also offers a potentially facile route for translation of optical imaging into the clinic. Essentially, the contrast agents are already widely used, and just appropriate optical equipment is required.

Recent work has sought to overcome the limited depth penetration of the UV/blue weighted Cerenkov luminescence using fluorescent agents. In this approach, small molecules and fluorescent nanoparticles are used to convert the Cerenkov light into longer and deeper penetrating wavelengths (secondary Cerenkov-induced fluorescence imaging; SCIFI).[7] However, this approach suffers from the same translational hurdles as the majority of optical molecular imaging approaches. It has used unapproved, and in some cases toxic materials (QDs) with biological and pharmacodynamic profiles that are not fully known. We previously have shown that we are able to convert Cerenkov light by shifting its wavelength through SCIFI, to enable activatable hybrid PET/Optical imaging.[8] However, direct modulation of the Cerenkov signal might have potential advantages

Here, we hypothesized that an alternative approach is to utilize absorptive optical contrast agents to modulate the Cerenkov radiation through quenching. Unlike fluorescent and luminescent agents, approved absorptive dyes are in widespread clinical use. The most common example is the vital dye, isosulfan blue, used in the sentinel lymph node biopsy

procedure to detect otherwise indistinguishable nodes.[9] Furthermore, an approved nanoparticle formulation ferumoxytol (Feraheme, AMAG) is also highly absorptive. In proof of concept systems, we demonstrate that absorptive small molecules and nanoparticles can be used to specifically absorb CL, to provide anatomically and molecularly specific contrast (**Figure 1B**). The use of combinations of clinical agents and their research analogues enable readout of biologically relevant parameters in addition to the radiotracer information implicit in Cerenkov imaging.

2. Cerenkov Quenching *in vitro*

Biological investigation of an absorptive-CL approach required biocompatible materials to be matched to the Cerenkov emitting tracer. In **Figure 2**, we show that the technique of CL modulation can be accomplished through quenching of signal using clinically applied materials, namely the patent blue dye Lymphazurin which is used in sentinel node biopsy procedures and iron oxide nanoparticles which have been approved as iron replacement drugs for anemia and off-label as MR contrast agents. Lymphazurin possesses a blue color and its strong optical absorbance results in even dilute solutions blocking much of the blue-weighted Cerenkov luminescence (Figure 2A,B). While the peak of the isosulfan blue compound is clearly red-shifted relative to the continuous Cerenkov radiation shoulder, the dye is such a potent light absorber that it effectively silences CL emissions. Using a concentration gradient of the dye, the light output acquired followed a dose-dependent fashion. However, the positron signal from [^{18}F]-FDG was unchanged (Figure 2C,D). This phenomenon can also be observed using small molecules specifically designed as fluorescent-dye quenchers. For example, the broadly absorbing Blackberry Quencher 650 was also an effective modulator of CL-signal (**Figure S1**).

Manipulation of the isosulfan blue dye for chemical modification or more advanced imaging is not possible. Nanoparticles offered the potential to significantly attenuate Cerenkov luminescence with greater absorptive properties on a per NP basis. Iron oxide NP have an absorbance profile that matches the Cerenkov spectrum closely, and are widely used as both a preclinical and clinical NP platform.[10] Ferumxytol (Feraheme, AMAG Pharmaceuticals), a clinically approved particle, was evaluated to show that the NP mediated Cerenkov absorbance can be achieved with the combination of two clinical agents: Feraheme and [^{18}F]-FDG. These two agents have clearly overlapping optical properties, suggesting that iron oxide nanoparticles are a powerful means to regulate CL detection. While the PET signal from co-mixed tracer remains constant, CL intensity is absorbed dose-dependently (Figure 2E-H).

3. Passive Accumulation for Cerenkov Quenching *in vivo*

In order to evaluate the use of iron oxide nanoparticles for use *in vivo*, we first investigated the passive accumulation of the NP at malignant sites. The preclinical SPIO NP were used, as their derivatization enables non-invasive corroboration of distribution with a complementary modality. In this case planar fluorescence imaging was used after modification of the SPIO with near infrared cyanine dye Cy5.5 (Cy5.5-SPIO; Schematic Fig. 2E). As a proof-of-principle, **Figure 3** illustrates the use of Cy5.5-SPIO administered

i.v. to nude mice bearing subcutaneous HT1080 xenografts to perform *in vivo* Cerenkov luminescence modulation.

The administered NP dose was equivalent to the recommended patient dose of ferumoxytol (by mass of iron), adjusted for the mass difference of the small animal. Accumulation of the particles through the enhanced permeability and retention (EPR) effect[11] was monitored by fluorescence at 24 h (Figure 3A). [^{18}F]-FDG was then injected i.v. and PET and CL imaging were performed (Figure 3B,C). The [^{18}F]-FDG uptake by PET revealed no statistical difference between animals injected with Cy5.5-SPIO or PBS. However, from CL region of interest (ROI) measurements, a significantly reduced average radiance was detected only in tumors of mice injected with Cy5.5-SPIO (Figure 3 D,E). Accumulation of the nanoparticles at the tumor, as visualized through the decrease in CL provides a means to gain information about the tumor microenvironment, in this case the leaky microvasculature surrounding these fast growing fibrosarcomas. This approach enables the acquisition of standard nuclear medicine scans of glucose metabolism by [^{18}F]-FDG, in addition to the nanoparticle derived quenching through NP accumulation.

4. Targeted in vivo Quenching of CL

Moving beyond reliance on the passive EPR effect, we proceeded to demonstrate quenching through active targeting *in vivo*. We sought to specifically target the human somatostatin receptor subtype-2 (hSSTr$_2$). This receptor is over-expressed on neuroendocrine tumors, and is targeted clinically using the hSSTr$_2$ agonist octreotate (OCT; D-Phe-cyclo(Cys-Tyr-D-Trp-Lys-Thr-Cys)-Thr)[12] for both diagnostic and therapeutic strategies of disease management. Conjugation to the NPs yielded Cy5.5-SPIO-OCT (**Figure S2**). Mice bearing C6 glioma xenografts expressing hSSTr$_2$ and the negative wild type cells were evaluated by [^{18}F]-FDG PET and then injected with Cy5.5-SPIO-OCT.[13]

One day after injection of the targeted NP at the clinical dose used for ferumoxytol, mice underwent fluorescence imaging to evaluate nanoparticle uptake (**Figure 4**). Immediately thereafter, [^{18}F]-FDG was administered and Cerenkov and PET signals were acquired (Figure 4B). The quantitative readout from PET enables determination of the glucose metabolism, through accumulation of the radioactive sugar. Because of greater glycolytic activity, we are able to detect nearly 33% higher [^{18}F]-FDG uptake in the hSSTr$_2$-positive tumors by CL and PET. However, when normalizing the light detected by the PET signal, it is not possible to discern the somatostatin-receptor expressing tumor.

Following injection of Cy5.5-SPIO-OCT, nuclear imaging was repeated after one day. Now, a specific and significant ($p < 0.05$) difference in normalized radiance can be detected. The site specific quenching of the Cerenkov signal at the hSSTr$_2$-expressing tumor provides means to noninvasively characterize the molecular profile of the xenograft. This is in addition to the quantitative information presented from a conventional PET scan. These results, in conjunction with the significantly attenuated Cerenkov signal in the hSSTr$_2$-positive tumor after targeted Cy5.5-SPIO-OCT uptake, highlight the feasibility of multiparameter non-invasive tumor marker imaging.

5. Conclusion

In conclusion, this work demonstrates that absorption of Cerenkov luminescence by small molecule and nanoparticle tracers is feasible. Furthermore, the utility of the strongly overlapping iron oxide nanoparticle absorption spectra and the Cerenkov radiation spectrum produced by [^{18}F]-FDG make iron oxide NP a potentially important multimodal tracer for this evolving field. Ongoing optimization of the nanoparticle-based Cerenkov quenching strategy is thus warranted. In this study, we had chosen to utilize materials at the clinical interface; [^{18}F]-FDG and analogs of ferumoxtyol, the FDA approved iron oxide nanoparticle. Previous work has already demonstrated the value of endogenous contrast generators such hemoglobin for Cerenkov imaging of the vasculature and oxygenation of tissue.[14] Independently, we have expanded that work with the large toolkit of absorptive passive and targeted molecular imaging probes for further visualization of disease relevant biology.

Other absorptive moieties could be used in the same fashion to generate the activatable contrast seen here both *in vitro*, and *in vivo*. Using passive or molecularly specific agents to exploit the quenching strategy *in vivo* in combination with experimental treatments would expand the pallet of biomedically relevant characteristics of disease that can be readout in a single imaging study. For example, the non-targeted NP strategy could be used to evaluate the effect of anti-angiogenic treatments as normalization of tumor vasculature should reduce the passive accumulation of the absorptive NP at the tumor leading to an increased optical signal. This is especially relevant as direct translational application is, unlike much nanoparticle work, eminently feasible. To underline this; through the results presented here, we have shown that with material directly from the clinical pharmacy, we are able to enhance our insight into tumor biology with preclinical multimodal imaging.

With the targeted approach, NP provide a means to gain information critical for disease management decisions. In addition to assessing glucose metabolism by [^{18}F]-FDG and PET, this technique is able to contribute to our knowledge of the tumor microenvironment, and specific ligand presentation that will help to molecularly characterize a lesion. There is also the potential that these methods can also be integrated with our recent success for activatable, secondary Cerenkov induced fluorescence imaging.[8] Using appropriate reversibly-activatable agents, such as molecular beacons that shift between a inactive (quenched) and active (fluorescent), the combination of quenching and secondary Cerenkov-induced fluorescence imaging could provide additional real-time information, that could possibly be utilized in a intraoperative setting [17] or via laparoscopy [18] to provide additional information for the operating surgeon.

6. Experimental Section

Chemicals, Radionuclides and Tracers

All materials were purchased from Thermo Fisher Scientific, unless otherwise noted. The amine-reactive cyanine5.5-N-hydroxysuccinimide (Cy5.5-NHS) was purchased from GE Healthcare. Peptide was obtained from Anaspec, Incorporated.

^{18}F-fluorodeoxyglucose ([^{18}F]-FDG) was supplied by IBA Molecular with a specific activity of >41 MBq/μmol (>11 mCi/μmol) and a radiochemical purity of >98%. The tracer was obtained through the Radiopharmacy of the Department of Nuclear Medicine at Memorial Sloan-Kettering Cancer Center (MSKCC).

Nanoparticle Probes

Ferumoxyol (Feraheme; AMAG Pharmaceuticals, Inc.) was used as provided. Cross-linked superparamagnetic iron oxide nanoparticles (SPIO) were synthesized as described previously.[14] Briefly, iron chlorides were precipitated to iron oxide through the addition of ammonia in a solution of dextran (Pharmacosmos). The particles were subsequently cross-linked and aminated by reaction with epichlorhydrin and ammonia and re-purified. Cy5.5-NHS was reacted in a 15:1 molar ratio with the particles in sodium bicarbonate buffer (0.1 M, pH 8.5). The final product, Cy5.5-SPIO, was purified using gel filtration chromatography (PD10; GE Healthcare).

Peptide-conjugated Cy5.5-SPIO was synthesized to target the human somatostatin receptor subtype-2 (hSSTr2). This was accomplished by reacting the Cy5.5-SPIO with 100× molar excess DSS in 1:1 DMF/DMSO for 30 min. The particles were quickly precipitated and resuspended in pH 8 citrate buffer containing 0.5 mg of octreotide acid (Octreotate; Anaspec, Inc). Particles were reacted for 4 h, washed on a PD10 column in pH 7.4 PBS and concentrated using a YM-50 filter. The coupling reaction schematic, found in **Figure S2**, was partly accomplished using the PyMOL Molecular Graphics System, Version 1.2r3pre, Schrödinger, LLC. Specific targeting of by Cy5.5-SPIO-OCT was determined using flow cytometry (MACS Quant, Miltenyi Biotec, Bergisch Gladbach, Germany). One million trypsinized hSSTr2-expressing and control WT cells (C6) were incubated for 30 minutes at 37 °C and 5% CO2 with nanoparticles, washed 3 times in PBS and analyzed. Mean fluorescence values using specific Cy5.5-SPIO-OCT were 9124 (C6-hSSTr2) and 413 (C6-WT). Mean fluorescence values using non-specific Cy5.5-SPIO were 215 (C6-hSSTr2) and 253 (C6-WT).

Animal Experiments

All animal experiments were conducted in compliance with Institutional Animal Care and Use Committee guidelines and the Guide for the Care and Use of Laboratory Animals.[16] All animal procedures were performed under anesthesia by inhalation of a 1-4% isoflurane-air mixture (Baxter Healthcare). Animals were obtained from Harlan Laboratories (Indianapolis, IN). Athymic Nu/Nu mice between the ages of 10 and 16 weeks were used for all experiments.

Spectrophotometry

All probes and radionuclides were characterized for absorbance and luminescent properties using a SpectraMax M5 (Molecular Devices, Sunnyvale, CA). All samples were read using a quartz cuvette (volumes between 250 and 1000 μL). Concentration measurements of the SPIO probes were obtained by acidic digestion of the probe and spectrophotometric assessment using a standard curve, as described.[15]

Cerenkov Luminescence (CL) Imaging

CL images were obtained using the IVIS 200 (Caliper Life Sciences). This system utilizes a cryo-cooled EMCCD for high sensitivity detection of low light sources. In vitro imaging: Cerenkov absorbance by Cy5.5-SPIO (concentration of iron ranging from 0.5 to 4 mg/mL) was determined using a cooled (−20 °C) cathode with dual microchannel plates, the XR/MEGA-10Z (Stanford Photonics, Palo Alto, CA). 1.85 MBq of [^{18}F]-FDG was added to each well. Without cosmic ray filtering, 30 frame per second images were summed for the 10 second acquisition and false-colored in ImageJ (NIH, Bethesda, MD). The identical protocol for Cerenkov absorbance of ferumoxytol and small molecules was conducted, except on the IVIS 200 instrumentation. In addition, a second low-light, high-sensitivity camera system was used to demonstrate acquisition of Cerenkov images on multiple devices. Namely, for Figure 2C, the Mega10Z intensifier charged coupled device camera was used (Stanford Photonics, Palo Alto, CA). This camera is a GaAsP dual microchannel-plate gain device with zero effective read noise and single photon counting capabilities. The device was run at 120 frames per second, with the final image integrated for the 1 min acquisition duration.

PET Imaging

Mice were imaged in a prone position using the R4 microPET™ dedicated small-animal PET scanner (Concorde Microsystems, Inc.), with an energy window of 350-700 keV and coincidence timing window of 6 ns. Images were acquired at 60 minutes post-administration over a period of 15 minutes.

The list-mode data were sorted into 2D histograms by Fourier re-binning and images reconstructed by filtered back-projection using a ramp filter with a cut-off frequency equal to the Nyquist frequency in a 128 × 128 × 64 matrix. Normalized image data (ie. corrected for non-uniformity of scanner response) was corrected for dead time count losses and physical decay to the time of injection.

Count rates in the reconstructed images were converted to activity concentration and subsequently percent of injected dose per gram of tissue (% ID/g) using a system calibration factor (μCi/mL/cps/voxel) derived from imaging a mouse-size phantom filled with a uniform aqueous solution of [^{18}F]-FDG. The reconstructed images were visually examined and analyzed using ASIProVM (Concorde Microsystems, Knoxville, TN) with window and level settings adjusted for maximal tumor visibility. ROI were manually drawn to circumscribe tumors. The mean %ID/g within the structure was computed from the VOI generated from ROI in sequential slices. For all [^{18}F]-FDG acquisitions, animals were deprived of food for between 4 and 6 h prior to imaging.

Fluorescence Imaging

Fluorescent images of mice were obtained on the Maestro animal imaging system (Caliper Life Sciences). Appropriate excitation and emission spectral filters were used. False color spectral deconvolution was set as follows: Red for Cy5.5-SPIO and Cy5.5-SPIO-OCT; Green for food and Blue for liver. For non-targeted quenching Cerenkov luminescence experiments, animals were imaged at the specified times, following 150 μL injection of 2.5

mg/mL Cy5.5-SPIO. Spectral unmixing of obtained image sets (using the Yellow filter) was performed using probe standards and low fluorescent food. The targeted Cy5.5-SPIO-OCT overlay of probe channel with white light image was performed in ImageJ.

Statistical Analysis

Statistical comparisons were made using the Student's *t*-test. All experiments were performed in triplicate unless otherwise indicated.

Supplementary Material

Refer to Web version on PubMed Central for supplementary material.

Acknowledgements

We thank the staff of the Radiopharmacy at MSKCC, Dr. Pat Zanzonico and the Small Animal Imaging Facility. Technical services provided by the MSKCC Small-Animal Imaging Core Facility was supported in part by NIH Cancer Center Support Grant No 2 P30 CA008748-48, NIH Shared Instrumentation Grant No 1 S10 RR020892-01 and a Shared Resources Grant from the MSKCC Metastasis Research Center, D.L.J.T. and this work were supported by US National Institutes of Health (NIH) through the R25T Molecular Imaging Fellowship: Molecular Imaging Training in Oncology (5R25CA096945-07; Prinicpal investigator H. Hricack). J.G. was supported by US Department of Defense (PC111667), and NIH (1R01EB014944–01) and a Louis V. Gerstner Young Investigator Award. Technical services provided by the Facility were supported in part by grants from NIH; R24 CA083084 and P30 CA08748.

References

1. Tsien RY. Nat. Rev. Mol. Cell Biol. 2003; 4:S1.
2. Ntziachristos V. Annu. Rev. Biomed. Eng. 2006; 8:1. [PubMed: 16834550] Massoud TF, Gambhir S. Genes. Dev. 2003; 17:5.
3. van Dam GM, Themelis G, Crane LMA, Harlaar NJ, Pleijhuis RG, Kelder W, Sarantopoulos A, de Jong JS, Arts HJG, van der Zee AGJ, Bart J, Low PS, Ntziachristos V. Nat. Med. 2011; 17:10. [PubMed: 21217660] Poellinger A, Burock S, Grosenick D, Hagen A, Lüdemann L, Diekmann F, Engelken F, Macdonald R, Rinneberg H, Schlag P-M. Radiol. 2011; 258:2.
4. L'Annunziata, MF. Radioactivity : introduction and history. Elsevier; Oxford, UK: 2007.
5. Robertson R, Germanos MS, Li C, Mitchell GS, Cherry SR, Silva MD. Phys. Med. Biol. 2009; 54:16.Cho JS, Taschereau R, Olma S, Liu K, Chen YC, Shen CK, van Dam RM, Chatziioannou AF. Phys. Med. Biol. 2009; 54:22.
6. Ruggiero A, Holland JP, Lewis JS, Grimm J. J. Nucl. Med. 2010; 51:7. [PubMed: 20008998] Liu H, Ren G, Miao Z, Zhang X, Tang X, Han P, Gambhir SS, Cheng Z. PLoS One. 2010; 5:3.
7. Dothager RS, Goiffon RJ, Jackson E, Harpstrite S, Piwnica-Worms D. PLoS One. 2010; 5:10.Lewis MA, Kodibagkar VD, Oz OK, Mason RP. Opt. Lett. 2010; 35:23.Liu H, Zhang X, Xing B, Han P, Gambhir SS, Cheng Z. Small. 2010; 6:10.
8. Thorek DL, Ogirala A, Beattie BJ, Grimm J. Quantitative imaging of disease signatures through radioactive decay signal conversion. Nat. Med. 2013; 19:10.
9. Giuliano AE, Kirgan DM, Guenther JM, Morton DL. Ann. Surg. 1994; 220:4.
10. Kircher MF, Mahmood U, King RS, Weissleder R, Josephson L. Cancer Res. 2003; 63:8.
11. Matsumura Y, Maeda H. Cancer Res. 1986; 46:12.
12. Reubi JC. Endocr. Rev. 2003; 24:4.Reubi JC, Schar JC, Waser B, Wenger S, Heppeler A, Schmitt JS, Maeke HR. Eur. J. Nucl. Med. 2000; 27:5.
13. Zhang H, Moroz MA, Serganova I, Ku T, Huang R, Vider J, Maecke HR, Larson SM, Blasberg R, Smith-Jones PM. J. Nucl. Med. 2011; 52:1. [PubMed: 21149477]

14. Axelsson J, Davis SC, Gladsotone DJ, Pogue BW. Med. Phys. 2011; 38:7.Steinberg JD, Raju A, Chandresekharan P, Yang C-T, Khoo K, Abastado J-P, Robins EG, Townsend DW. EJNMMI Res. 2014; 4:15. [PubMed: 24606872]
15. Thorek DLJ, Tsourkas A. Biomaterials. 2008; 29:26.
16. Institute of Laboratory Animal Resources (U.S.). Committee on Care and Use of Laboratory Animals. Guide for the care and use of laboratory animals. U.S. Dept. of Health and Human Services, Public Health Service; Bethesda, Md.: NIH publication
17. Holland JP, Normand G, Ruggiero A, Lewis JS, Grimm J. Mol. Imaging. 2011; 10:3. [PubMed: 21303611]
18. Liu H, Carpenter CM, Jiang H, Pratx G, Sun C, Buchin MP, Gambhir SS, Xing L, Chen Z. J. Nucl. Med. 2012; 53:10.

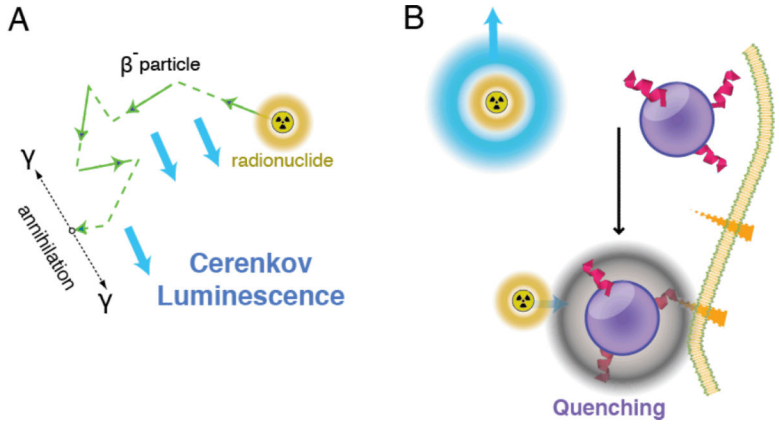

Figure 1.

Nanoparticle quenching of Cerenkov Luminescence. (A) CL can be produced by charged particles, for example those produced upon decay of PET-radionuclides, traveling at high speed through biological media. (B) Radionuclides at the disease site can produce detectable CL; for example [^{18}F]-FDG uptake by tumor cells. With nanoparticle colocalization through enhanced permeability and retention or targeted nanoparticle absorbers the CL signal is quenched. This enables dual readout of disease biology with non-invasive diagnostic imaging tools that are currently in wide-spread use.

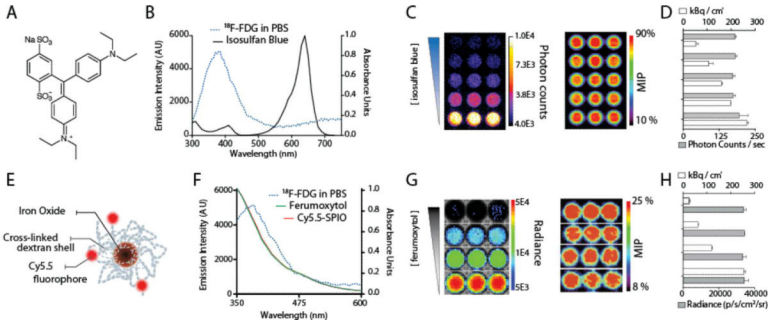

Figure 2.

Cerenkov Quenching with Clinical Applied Materials. (A) Chemical structure of the patent blue dye Lymphazurin, used for sentinel lymph node imaging. (B) CL profile and absorption spectra of [^{18}F]-FDG and patent blue dye, respectively. (C,D) Dose-dependent quenching of CL signal by Lymphazurin; PET signal remains unaffected. (E) Schematic of iron oxide nanoparticle, modification with fluorescent dyes. (F) CL profile of [18F]-FDG and absorption spectra of the FDA-approved ferumoxytol and the research grade Cy5.5-SPIO. (G,H) Again, a concentration gradient of the ferumoxytol produces a change in the amount of the CL signal produced, while PET signal remains constant. MIP, mean intensity projection of the tomographic PET dataset. Photon counts are counts/sec; Radiance units are photons/cm^2/sr/sec.

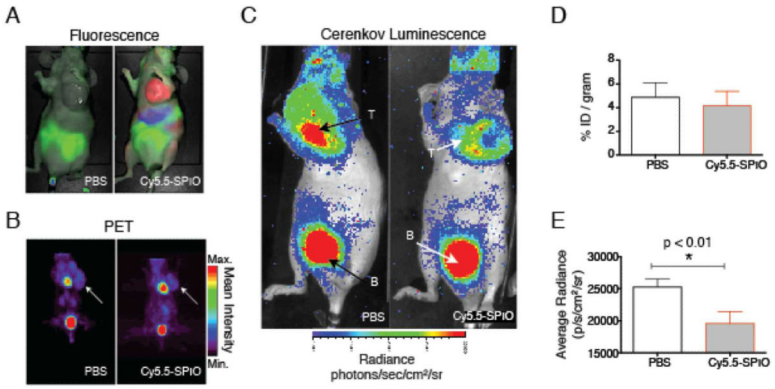

Figure 3.

In vivo Quenching of Cerenkov Luminescence with Iron Oxide Nanoparticles. The ferumoxytol analog, fluorescently labeled crosslinked iron oxide (Cy5.5-SPIO), or phosphate buffered saline (control) were administered to HT1080 tumor bearing mice. (A) Conventional fluorescent imaging of the Cy5.5 label (external excitation, color-coded in red) was used to follow probe accumulation. Food, green. (B) Following 24 h of nanoparticle uptake, [^{18}F]-FDG (14.8 MBq) was administered. Representative PET scans show equivalent tumor uptake. (C) The CL scans reveal differences in the light emitted from each tumor. There is greater light output from the PBS control injected mice. B; Bladder. (D) PET quantitation reveals no difference in [18F]-FDG uptake. (E) However, the Cerenkov luminescence detected in the tumors of mice given the Cy5.5-SPIO was significantly attenuated.

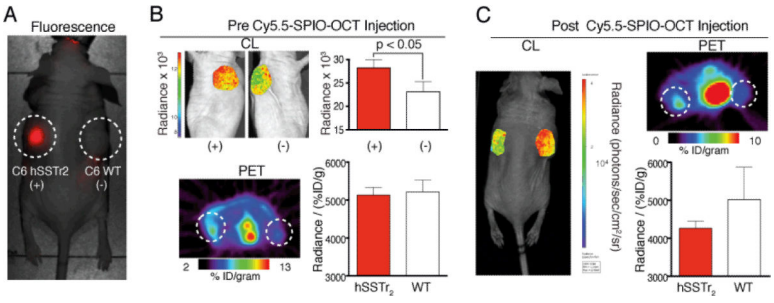

Figure 4.

Octreotate Modified Iron Oxide NP for Targeted Cerenkov Quenching. OCT-Cy5.5-SPIO were administered to mice bearing bilateral xenografts with (C6 $hSSTr_2$) or without (C6 WT) $hSSTr_2$ expression. (A) The fluorescent nanoparticles demonstrate the specific uptake of this new probe at the positive, hSSTR2-expressing, tumor. (B) Prior to nanoparticle administration, 11.1 MBq of [18F]-FDG was given for PET and CL imaging. Greater glycolytic activity in the $hSSTr_2$+ tumor CL of a representative animal is presented in left and right sagittal views with axial PET through the tumors. CL when normalized for percent injected dose per gram of [^{18}F]-FDG, is not significantly different between the two tumor types. (C) One day following dosing with Cy5.5-SPIO-OCT, the imaging was repeated. Now we are able to again obtain the quantitative information from functional PET imaging, but with the targeted quenching NP we are also able to add a layer of molecularly specific information to distinguish the tumors.